Orchestrating Composite Applications at the Edge

Surface & Coatings Technology 470 (2023) 129824

Contents lists available at ScienceDirect

Surface & Coatings Technology

journal homepage: www.elsevier.com/locate/surfcoat

Full length article

Coating of bioactive glasses with chitosan: The effects of the glass composition and coating method on the surface properties, including preliminary in vitro results

S. Spriano [a,*], G. Riccucci [a], G. Örlygsson [b], C.H. Ng [c], E. Vernè [a], F.P. Sehn [d], P.T. de Oliveira [d], S. Ferraris [a]

[a] Politecnico di Torino, Torino, Italy
[b] Ice Tec, 112 Reykjavik, Iceland
[c] Genis hf., Adalgata 34, 580 Siglufjördur, Iceland
[d] School of Dentistry of Ribeirão Preto, University of São Paulo, Ribeirão Preto 14040-904, SP, Brazil

ARTICLE INFO

Keywords:
Bioactive glass
Chitosan
Coating
Surface properties
Surface modification
In vitro tests

ABSTRACT

Two bioactive glasses were coated with chitosan: SCNB belongs to the SiO_2-CaO-Na_2O system, and SCNA has the addition of Al_2O_3 to enhance chemical stability. Different coating methods were compared: direct physical attachment, surface activation through tresyl chloride, and polydopamine as a linker. The samples were characterized through SEM-EDS, contact angle measurements, FTIR, zeta potential titrations, tape tests, in vitro precipitation of hydroxylapatite (bioactivity), and cell cultures (RAW 264.7 and UMR-106) on some selected samples. Direct physical attachment (in acetic acid) or use of polydopamine allowed complete surface coverage, while it dropped to one-quarter on both glasses by using tresyl chloride. The coating had a contact angle of about 80° and it well showed typical functional groups (FTIR). The coatings on SCNA were chemically and mechanically stable (classified as 4-5B by the tape tests, partially maintained after soaking for 14 days), and showed an isoelectric point around 8. On SCNB, the coatings were unstable (classified as 0-3B, dissolved during soaking) but bioactivity was preserved. The coating affected the biological outcome of SCNA with M0/M1 polarization (1 day) and reduced viability of macrophages (3 days), while osteoblastic cells showed poor adhesion but maintained cell viability and osteogenic potential (3–7 days).

1. Introduction

Bioactive glasses (BGs) are widely studied for their ability to induce bone healing due to their osteoconduction and osteoinduction properties. They are used for applications in the field of bone tissue regeneration due to their tailorable chemical composition that promotes, once they come into contact with the physiological fluids, the release of Na^+ and Ca^{2+} ions that are exchanged with H_3O^+ coming from the solution. This ion exchange causes the formation of a hydrated silica gel on the BG surface, which, in contact with extracellular fluids, rapidly turns into an amorphous CaO-P_2O_5-SiO_2 layer. A further evolution produces a crystalline hydroxycarbonate apatite layer which mediates the colonization, proliferation, and differentiation of osteoblasts [1].

The first BGs formulations were designed by L.L. Hench and his coworkers, who studied different compositions based on the SiO_2–Na_2O–CaO–P_2O_5 oxide system, selecting the composition $45SiO_2$–$24.5Na_2O$–$24.5CaO$–$6P_2O_5$ (wt%), referred to as 45S5 (trademarked by the University of Florida with the name Bioglass®), characterized by high amounts of Na_2O and CaO and a high CaO/P_2O_5 ratio, making the BG surface very reactive in the physiological environment [2].

BGs belonging to the ternary system SiO_2-CaO-Na_2O were thoroughly studied in the past by Kokubo and coworkers, who investigated the bioactivity (in vitro precipitation of hydroxylapatite) of P_2O_5-free silicate glasses [3,4]. This ternary composition was subsequently studied by Verné and coworkers to prepare bioactive glass-ceramic matrix composites [5] as well as antibacterial bioactive glasses [6], comparing glass compositions with different mechanical properties and bioactivity

* Corresponding author.
E-mail addresses: silvia.spriano@polito.it (S. Spriano), giacomo.riccucci@polito.it (G. Riccucci), ngchw@genis.is (C.H. Ng), tambasco@usp.br (P.T. de Oliveira), sara.ferraris@polito.it (S. Ferraris).

https://doi.org/10.1016/j.surfcoat.2023.129824
Received 14 June 2023; Received in revised form 11 July 2023; Accepted 20 July 2023
Available online 28 July 2023

indices, i.e. different rates of reactivity in simulated body fluid, for different applications.

Chitin is a linear polysaccharide with β-(1,4)-linkage abundantly available in nature. Chitosan is the deacetylated and more reactive form of chitin. The linear structure and exposure of amine groups are the key properties that make chitosan a highly versatile material available in different forms, such as nanoparticles, nanofibers, films, and hydrogels [7]. Additionally, due to its nontoxic and antimicrobial properties, bioresorbable and polycationic nature, and great potential in tissue regeneration, chitosan is widely applied in the pharmaceutical and medical fields. These include wound dressing, as an antimicrobial agent, in the controlled release of drugs, as a blood anticoagulant, and in tissue engineering, including nerve and bone regeneration [8–10]. Another important property of chitin/chitosan scaffolds is the promotion of cell proliferation and differentiation. Chitosan-based scaffolds can maintain cell activities and activate tissue regeneration [11].

Numerous trials have been conducted on the anti- and pro-inflammatory properties of chitosan and its derivatives, but the exact mechanism is not exactly understood, yet. Chang et al. [12] reported the use of chitosan in the range of 3.3 to 300 kDa to affect the NO secretion, cytokine production, and mitogen-activated protein kinase pathways in lipopolysaccharide (LPS)-induced murine RAW 264.7 macrophages. Davydova et al. [13] examined the anti-inflammatory activity of high (MW: 115 kDa) and low molecular weight (MW: 5.2 kDa) chitosan and concluded that the main contribution to the anti-inflammatory activity of chitosan is independent of its molecular weight but is driven by structural elements comprising the molecule. Both chitosan samples showed an increased induction of anti-inflammatory IL-10 cytokine in contact with animal blood and a down-regulation of colitis progress. Low deacetylation degree chitosan oligosaccharides protect against IL-1β induced inflammation and enhance autophagy activity in human chondrocytes [14]. Oberemko et al. [15] examined chitosan samples from two mushroom species and concluded that low-molecular-weight chitosan films and solutions with a high degree of deacetylation are cytotoxic on both tumor MH-22A and normal CHO cells in vitro.

During the last three decades, chitosan has been extensively studied in bone tissue engineering. Chitosan may act alone, or it can be blended with other polymers and natural or synthetic materials, which is generally considered an effective way to develop tissue engineering. In vivo studies by Pang et al. [16] and Ho et al. [17] showed that chitosan alone was sufficient to stimulate osteogenesis. Additionally, tissue regeneration processes can be further stimulated by the addition of drugs that influence cellular function and tissue regeneration; or the incorporation of materials, such as calcium phosphates, to facilitate partial mechanical supports and bone regeneration [18,19]. In all these efforts, the aim was to reproduce the biomechanical properties of natural bone [20].

The present study was designed to investigate the effects of different bioactive glasses compositions and coating procedures on the formation of a chitosan coating. This is why a more stable bioactive glass (SCNA) was compared to a more reactive one (SCNB), in addition, the direct physical attachment by dissolving chitosan in different solvents (acetic acid or PBS) was compared to the use of a surface activator (tresyl chloride) or a linker (polydopamine dissolved in water or PBS). SCNA was selected for its simple composition, good mechanical properties, and high stability, as reported in previous works concerning its silver surface enrichment on bulk and coatings [21,22] as well as surface functionalization with alkaline phosphatase and bone morphogenetic proteins [23–26]. SCNB was chosen for its high reactivity and has been designed by modifying the compositions of different bioactive glasses based on the silica-soda-lime system developed in previous studies and served to investigate the intrinsic antioxidant activity of silica-based bioactive glasses [27].

2. Materials and methods

2.1. Bioglass preparation

Two silica-based bioactive glasses were used: SCNA and SCNB. The composition of SCNA was 57.0 mol% (56.98 wt%) SiO_2, 34.0 mol% (31.72 wt%) CaO, 6.0 mol% (6.20 wt%) Na_2O, and 3.0 mol% (5.10 wt%) Al_2O_3 [23]. The composition of SCNB was 55.6 mol% (55.99 wt%) SiO_2, 21.7 mol% (23.62 wt%) CaO, and 22.7 mol% (20.39 wt%) Na_2O [28].

Glass round bars (10 mm in diameter) were obtained by the melt/quench process in a platinum crucible at 1550 °C for 1 h for SCNA and at 1450 °C for 2 h for SCNB. The molten glass was cast into a brass mold preheated at the temperature of annealing: SCNA was annealed at 600 °C for 10 h and SCNB at 520 °C for 6 h. The bars were cut into 2 mm thick slices with a diamond blade (IsoMet High Speed Pro, Buehler). Polishing was performed with abrasive SiC papers (120–4000 grit). Before functionalization, the surface hydroxyl groups of the bioactive glasses were exposed by washing in an ultrasonic bath, once in acetone for 5 min, and three times in deionized water, and drying at room temperature [24,25].

2.2. Functionalization with chitosan

The chitosan polymer was supplied by Genis hf. (Siglufjörður, Iceland). Acetic acid, hydrochloric acid, phosphate-buffered saline (PBS), NaOH, tresyl chloride, dopamine hydrochloride, and tris(hydroxymethyl)aminomethane (Tris) were obtained from Sigma-Aldrich.

2.2.1. Method 1 – direct physical attachment

Two procedures were tested to directly attach chitosan to bioactive glasses: dissolution of chitosan in acetic acid and suspension of chitosan in neutral PBS. The coated samples were stored in a desiccator.

In the first procedure, 0.75 %, and 1.5 % w/v chitosan was dissolved in 1 % v/v acetic acid. The bioactive glass specimens were immersed into the 0.75 % solution for 5 min and then dried overnight at room temperature in air (under a hood). The specimens were neutralized in a solution of 1 M NaOH for 1 h and then washed three times with deionized water. The specimens treated this way were denoted as SCNA-AA and SCNB-AA.

In the second procedure, a 1.0 % w/v suspension of chitosan in PBS with pH 7.32 was prepared and mixed for 5 min in a syringe. The concentration of dissolved chitosan was limited under the given conditions and thus mostly present in suspension. The bioactive glass specimens were immersed into the suspension for 5 min at 36 °C in an incubator and then dried at room temperature. The specimens were denoted as SCNA-PBS and SCNB-PBS.

2.2.2. Method 2 – tresyl chloride activation

Tresyl chloride was used to convert the surface hydroxyl groups of the bioactive glasses into sulfonyl ester groups which represent a good chemical leaving group. The specimens were covered with tresyl chloride and stored at 37 °C for 24 h. Subsequently, the samples were washed with deionized water, a solution of deionized water plus acetone (50:50), and acetone. A suspension of chitosan in PBS was prepared, as described above, and the specimens were immersed in the solution for 24 h at room temperature. After the immersion, the specimens were rinsed three times with deionized water, dried at room temperature, and stored in a desiccator. The specimens treated this way were denoted as SCNA-TC-PBS and SCNB-TC-PBS.

2.2.3. Method 3 – polydopamine treatment

Polydopamine is spontaneously formed by pH-induced oxidative polymerization of dopamine hydrochloride in an alkaline solution (pH $>$ 7.5). 2 mg/ml dopamine hydrochloride solution was prepared by dissolving dopamine hydrochloride in a 10 mM Tris solution and adjusting pH to 8.5 with HCl. The bioactive glass specimens were soaked

in the dopamine hydrochloride solution for 4 h at room temperature under continuous stirring. After the soaking, the specimens were rinsed with deionized water and dried at room temperature. 1 % w/v chitosan was dispersed in deionized water or PBS. The polydopamine-soaked specimens were incubated in these solutions for 24 h under stirring at room temperature to obtain specimens denoted as SCNA-PD-W, SCNA-PD-PBS, SCNB-PD-W, and SCNB-PD-PBS.

2.3. Characterization of samples

A Zeiss Supra 25 FE-SEM scanning electron microscope (SEM) was used to investigate the as-prepared samples. A JEOL JCM-6000PLUS was used for SEM observation of the coated samples after the tape test. Before observation, the samples were gold-coated in a sputter coater S150B (Edwards). The surface morphology was visualized with the SEM and image analysis (Image J - Rasband, W.S., ImageJ, U. S. National Institutes of Health, Bethesda, Maryland, USA) was used to quantify the degree of the surface coverage by the chitosan coating. The expected penetration depth was calculated by using the Potts equation [29].

Water contact angles were determined using a KSV CAM200 optical contact angle meter (KSV Instruments) and a droplet volume of 5 μl deionized water. The contact angle measurement was started 15 s after drop-down and calculated using the Laplace & Young equation. Measurements were performed at room temperature and ambient humidity. 5 measurements were performed for each specimen.

Zeta potential titration curves as a function of pH were obtained by means of electrokinetic measurements (SurPASS, Anton Paar). Two samples were positioned face to face in an adjustable gap cell at a distance of 100 μm and a 0.001 M KCl electrolyte solution, with a starting pH of 5.6, was fluxed between the surfaces. The pH was varied by adding 0.05 M HCl or 0.05 M NaOH. 4 measurements were acquired for each pH value. The basic and acidic ranges were measured through two separate measurements both starting from pH 5.6 on the same set of samples. The basic range was measured first in order to obtain an eventual detrimental swelling of the chitosan coating only at the end of the measurement.

The tape test was performed according to ASTM D3359-17 [30] to measure the adhesion of the coatings to the substrates. A grid of parallel cuts was prepared on each specimen, the surface was gently cleaned with a brush, and the tape was fixed to the surface and then removed to test the coating adhesion. Subsequently, the surface was inspected by optical microscopy and SEM, and compared with the reference schemes reported in the standard, to estimate the coating removal within the areas delimited by the grid.

2.4. Bioreactivity in SBF

Selected samples were incubated in a simulated body fluid (SBF). The chemical composition and procedure for the preparation are described in [31]. Samples were soaked for 2 weeks at 37 °C in order to test the stability of the coatings, in an environment close to physiological conditions, and to monitor potential hydroxylapatite formation on the specimen surfaces. SBF was renewed every two days. The samples were subsequently characterized by SEM. The specimens incubated were SCNA, SCNA-AA, SCNA-PD-W, SCNB, SCNB-AA, and SCNB-PD-W.

2.5. Biological tests

2.5.1. Osteoblastic and macrophage cell cultures

Rat osteoblastic UMR-106 cells (ATCC® CRL-1661™, American Type Culture Collection, Manassas, VA, USA) [32] were plated at a density of 20,000 cells/well on either SCNA or SCNA-AA discs placed in 24-well polystyrene plates (Corning Inc.) and cultured in Dulbecco's Modified Eagle Medium (D-MEM, Invitrogen, Carlsbad, CA, USA) supplemented with 10 % fetal bovine serum (Invitrogen), 50 μg/ml gentamicin (Gibco, Invitrogen), 50 μg/ml vancomycin (Gibco, Invitrogen), and 0.3 μg/ml fungizone (Gibco, Invitrogen), 50 μg/ml ascorbic acid (Sigma-Aldrich, St. Louis, MO, USA), and 7 mM beta-glycerophosphate (Sigma-Aldrich) for up to 7 days. Mouse macrophage RAW 264.7 cells (ATCC® TIB-71™) were plated and cultured under the same conditions (but without osteogenic supplements) for up to 3 days [33]. Both cell lines were maintained at 37 °C in a humidified atmosphere containing 5 % CO_2 and 95 % atmospheric air, and the culture medium was changed every 2–3 days. Cell growth was visualized on polystyrene using an Axiovert 25 inverted phase microscope (Zeiss Inc., Göttingen, Germany).

2.5.2. Cell and culture morphology by epifluorescence

On day 1 of RAW 264.7 cultures and day 3 of UMR-106 cultures on SCNA and SCNA-AA discs, cells were fixed in 4 % paraformaldehyde in 0.1 M phosphate buffer (PB; pH 7.2) at room temperature (RT), and then permeabilized using Triton X-100 at 0.5 % in PB. RAW 264.7 cells were labeled with an anti-osteopontin monoclonal antibody (MPIIIB10-1, 1:800, Developmental Studies Hybridoma Bank (DSHB), Iowa City, IA, USA), whereas UMR-106 cells were labeled with an anti-bone sialoprotein monoclonal antibody (WVID1-9C5, 1:200, DSHB). Both cell lines were then also labeled with Alexa Fluor 488-conjugated phalloidin (1:200, InvitrogenTM A12379), for the actin cytoskeleton, and 4′,6-diamidino-2-phenylindole, dihydrochloride (DAPI) (300 nM, Molecular Probes, Eugene, OR, USA), for nuclei [34]. Glass coverslips (Fisherbrand, Thermo Fisher Scientific, Waltham, MA, USA) were mounted on the surface containing the cells with Vectashield anti-fade fluorescence mounting medium (Vector Laboratories, Burlingame, CA, USA). All samples were then examined in an Axio Imager 2 fluorescence microscope (Carl Zeiss, Jena, Germany) coupled to an AxioCam MRm digital camera (Carl Zeiss). Images were acquired using the AxioVision 4.8.2 program and processed in Adobe Photoshop CS5 (Adobe Systems, San Jose, CA, USA).

2.5.3. Cell metabolic activity/cell viability assay

On hour 6 and day 3 of RAW 264.7 cultures, and day 3 of UMR-106 cultures on SCNA and SCNA-AA discs, cell metabolic activity/viability was assessed by the {[3-(4,5-dimethylthiazol-2-yl)-2,5-diphenyltetrazolol] bromide} (MTT) colorimetric assay (Sigma-Aldrich) [35]. Briefly, cells were incubated in culture medium +10 % MTT for 4 h at 37 °C, in a humidified atmosphere containing 5 % CO_2 and 95 % atmospheric air. The culture medium was then removed, and 1 ml acidic isopropanol solution (Merck, Darmstadt, Germany) was added to each well under stirring for 5 min, for complete solubilization of the formed precipitate. Then, 150 μL aliquots were transferred to a 96-well plate for reading on a spectrophotometer (μQuanti, BioTek Instruments Inc., Winooski, VT, USA) at a wavelength of 570 nm.

2.5.4. Mineralization of osteoblastic cell cultures

On day 7 of culture, UMR-106 cells grown on SCNA or SCNA-AA discs were fixed in 70 % ethanol at 4 °C for 60 min and stained with 2 % Alizarin Red (Sigma-Aldrich), pH 4.2, at RT for 15 min. Alizarin Red extraction [36] was carried out under stirring for 30 min after adding 280 μL of 10 % acetic acid to each well. The cell layer was removed, and the samples were then heated to 85 °C, cooled on ice, and centrifuged. Then, 100 μL of each supernatant was added to 40 μL of 10 % NH_4OH, and the samples were read on a spectrophotometer (μQuanti, BioTek Instruments Inc.) using a 405 nm wavelength. The standard curve was obtained by the successive dissolution of Alizarin Red in ammonium acetate ($NH_4CH_3CO_2$).

2.6. Statistical analyses

The statistical analyses were carried out using GraphPad Prism software 8.3.0 (GraphPad Software Inc., San Diego, CA, USA). The quantitative data obtained with MTT and Alizarin Red assays were first subjected to the Shapiro-Wilk normality test. Then, two-way ANOVA,

followed by Tukey's post hoc test, was applied to the MTT assay for RAW 264.7 cells, and an unpaired *t*-test to Alizarin Red assay for UMR-106 cells. The non-parametric Mann-Whitney test was applied to the MTT assay for UMR-106 cells. Parametric data are presented as mean and standard deviation (SD), and non-parametric data as the median and interquartile range (IQR) of four experimental replicates in one biological replicate. The level of significance was set at 5 %.

3. Results and discussion

3.1. SEM and EDS analysis

The first evaluation of the coatings was based on SEM observations and results are reported in Fig. 1. The activated glasses (substrates) were used as a reference; they were washed to enhance surface hydroxylation and coating adhesion as described in the Materials and methods section and in Refs. [24, 25]. The covered area was quantified by image analysis and the results are reported in Table 1, where the EDS analyses are also reported. A low magnification was selected to get an overview of the coated surfaces and some enlargements were added when a more detailed observation was needed (see Fig. 1e, f). The EDS analyses were performed by scanning an area; data are marked with an asterisk when the coating was sporadic and the analyses were performed on a point within a covered area.

Few unavoidable morphological surface defects were observed on the bare glasses (Fig. 1a–b). Experimental EDS analyses of the bare glasses can be compared to the nominal compositions. The experimental Na/Ca ratio was 0.20 (SCNA) or 1.10 (SCNB) which was very close to the nominal compositions. The same was for the experimental Si/Ca ratio (1.26 for SCNA and 1.82 for SCNB). In conclusion, the experimental compositions of both glasses corresponded to the nominal ones.

The surface of SCNA-AA (Fig. 1c) was quite homogeneous and the EDS analysis clearly showed the presence of an organic coating on the glass surface. An evident increase of carbon (from 5 % up to about 45 %) and nitrogen (from undetectable up to 5 %) was detected with respect to SCNA, and the absence of the glass elemental components (aluminum, calcium, and silicon). The presence of sodium was slightly increased with respect to SCNA, but it could derive from the acid neutralization in NaOH after the coating formation. The quantitative image analysis gave a value of almost 100 % of surface coverage. The EDS beam penetration deduced from the acceleration voltage (5 kV) and chitosan density (0.9 g/cm^3) was about 1.2 μm. It can be deduced that the chitosan layer was thicker than the maximum penetration depth of the beam. Hence, the high solubility of chitosan at acidic pH (in acetic acid) had a positive outcome in the direct physical attachment of chitosan to SCNA.

When the solvent was changed, the result was different. The morphology of SCNA-PBS was not uniform and the coverage area was reduced by about 50 %. Chitosan did not form a continuous layer, but large agglomerates were visible (see the enlargement in Fig. 1e) so that the glass surface was visible. EDS analysis of the clearly covered areas (Table 1) revealed that the chemical composition of the chitosan coating was analogous to SCNA-AA. The presence of chloride may be due to the use of PBS. The low solubility of chitosan at neutral pH (in PBS) affected negatively the outcome of direct physical attachment. The formation of agglomerates was observed also in the chitosan-PBS suspension.

An even worse result was obtained by using tresyl chloride as a surface activator. The SEM image (Fig. 1g) shows a discontinuous coating, the surface coverage was about 25 %, and the elements characteristic of the SCNA glass were clearly detectable (in a reduced amount compared to SCNA) even if the EDS analysis was performed on a point inside a covered area. This result revealed that a higher surface reactivity was insufficient to solve the issue coming from the limited solubility of chitosan in PBS. The coating of the tresylated substrates by solubilizing chitosan in acetic acid was not explored because the amino groups on chitosan are protonated in acetic acid and this prohibits the nucleophilic attack of the amino functional group necessary to displace the tresyl leaving group and to form a bond with the surface.

Encouraging results were obtained by using polydopamine as a linker. SCNA-PD-W (Fig. 1i) and SCNA-PD-PBS (Fig. 1m) had a high surface coverage of 74 % and 94 % respectively and high carbon and nitrogen values. By this method, chitosan was dispersed in water or PBS to not damage the pre-coating with polydopamine. Chitosan dissolved in acetic acid cannot be used to coat the polydopamine-modified surfaces because an acidic environment inactivates the chitosan amino functional groups with respect to bond-forming with the polydopamine functional groups. PBS showed to be a good dispersant for this method, better than water because the coating was formed by covalently linking the well-dispersed fraction of chitosan without any precipitation of the less dispersed fraction.

Another comparison can be done by changing the substrate and using

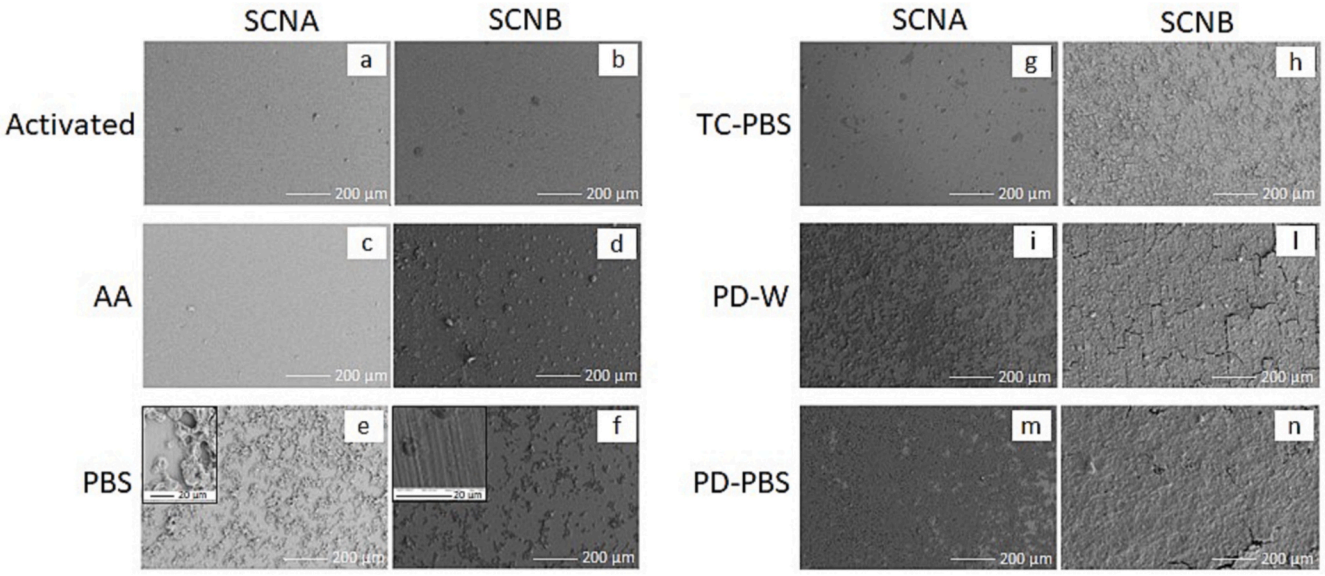

Fig. 1. SEM micrographs of the substrates (activated SCNA and SCNB glasses – a, b) and chitosan-coated samples: direct physical attachment by dissolving chitosan in acetic acid (c, d) or PBS (e, f); surface activation with tresyl chloride and chitosan dissolved in PBS (g, h); polydopamine linker with chitosan dissolved in water (i, l) or PBS (m, n).

Table 1
EDS analysis of the bare SCNA and SCNB glasses and chitosan-coated samples. The data refer to area analyses except when they are marked with an asterisk: in this case, the analysis was on a point within the covered area. The surface coverage calculated by using image analysis was also reported.

Element (sigma)	SCNA	SCNB	SCNA-AA	SCNB-AA	SCNA-PBS*	SCNB-PBS*	SCNA-TC-PBS*	SCNB-TC-PBS*	SCNA-PD-W	SCNB-PD-W	SCNA-PD-PBS	SCNB-PD-PBS
C (0.48–1.12)	5.20	5.80	44.57	34.64	51.89	56.13	41.62	45.23	58.91	57.15	54.61	50.16
N (0.51–1.01)	–	–	7.5	4.24	8.62	9.07	–	6.08	9.90	9.74	8.55	7.95
O (0.37–1.10)	42.0	39.26	40.72	43.48	25.74	17.86	26.52	43.98	31.19	33.11	36.84	40.68
Na (0.11–0.41)	4.02	15.42	7.21	3.31	4.60	8.94	2.5	1.15	–	–	–	1.21
Si (0.22–0.50)	25.80	25.53	–	14.34	–	1.01	12.83	–	–	–	–	–
Ca (0.16–0.21)	20.41	13.99	–	–	–	–	11.80	–	–	–	–	–
Al (0.07–)	2.56	–	–	–	–	–	1.71	–	–	–	–	–
Cl	–	–	–	–	9.15	6.99	–	–	–	–	–	–
P (1.20)	–	–	–	–	–	–	–	3.56	–	–	–	–
Surf. coverage [%]	–	–	99.8	100	52.9	51.6	25.7	27	73.5	96.2	93.8	93.8

a more reactive bioactive glass: SCNB. This glass does not contain alumina, its surface easily reacts in aqueous media to form a silica gel, and it induces hydroxylapatite precipitation in a faster way than SCNA when soaked in SBF [23,28]. Looking at the surface morphology (Fig. 1d, f, h, l, n) and surface coverage (Table 1), a similar trend of the efficacy of the different coating methods can be observed: formation of a continuous layer of chitosan and high surface coverage by using direct physical attachment in acetic acid (Fig. 1d) or polydopamine as a linker (Fig. 1l–n), a halved covering by using direct physical attachment in PBS (Fig. 1f), and the least complete covering on the tresylated substrate (Fig. 1h). Some differences to SCNA can be observed in the morphology of the coatings. By using direct physical attachment in acetic acid, some rounded protrusions could be observed on SCNB-AA (Fig. 1d), while the glass substrate appeared modified by a chemical reaction in the uncovered areas of SCNB-PBS (Fig. 1f) and cracks were present on SCNB-PD-W (Fig. 1l) and SCNB-PD-PBS (Fig. 1n). All these differences can be ascribed to the surface reactivity of SCNB that is enhanced at neutral-alkaline pH. Where the reaction occurred (such as on the rounded protrusion of SCNB-AA) EDS evidenced a higher amount of calcium and this suggests that the reaction involved a partial dissolution of silica and sodium oxide.

The presence of the coatings on the different samples was confirmed by FTIR analysis as reported in Fig. 1S (Supplementary Information).

3.2. Wettability

The water contact angles measured on the bare and coated surfaces are reported in Table 2.

A low contact angle was measured on the bare (washed) glasses because of the expected high exposure of OH groups which results in a remarkable wettability. As expected, the contact angle was lower on SCNB (about 10°) than on SCNA (about 30°) because of surface hydroxylation.

Chitosan is expected to be hydrophobic and thus increases the surface contact angle. Coating by using physical attachment in acetic acid resulted in a contact angle close to 80° for both glasses. This value was considered a reference for a homogeneous and smooth chitosan coating. Otherwise, the contact angles of the samples coated by physical attachment in PBS decreased because of the non-uniform coating. In this case, the water droplet was partially in contact with the glass substrates during the measurement. Then, high roughness due to agglomeration of chitosan (Fig. 1e–f) could influence the contact angle, too. A similar conclusion was drawn for SCNA-TC-PBS and SCNB-TC-PBS which were only partially coated (contact angle around 60°). In this case, the wettability was measured even on the tresylated (not yet coated) substrates. The obtained contact angles were not reported because they were too low to be measured (almost 0°). The super-hydrophilicity of the tresylated substrates evidenced an effective surface activation.

Table 2
Water contact angles measured on the bare SCNA and SCNB glasses and chitosan-coated samples.

		AA	PBS	PD_W	PD_PBS	TC_PBS
SCNA	31.5 ± 4	77.1 ± 3	51.2 ± 9	99.4 ± 6	69.2 ± 5	61.6 ± 9
SCNB	23.0 ± 2	82.0 ± 6	65.1 ± 8	74.2 ± 4	46.0 ± 5	64.0 ± 7

In the case of the samples coated with polydopamine as a linker, the measured contact angles were quite different compared to SCNA-AA and SCNB-AA. As a control, the contact angles on the substrates soaked in polydopamine (without the chitosan coating) were also measured (not reported) and they resulted in values similar to those of untreated glasses. An effect of surface roughness, partial uncovering, and cracks can explain the observed differences of SCNA-PD-W, SCNA-PD-PBS, SCNB-PD-W, and SCNB-PD-PBS with respect to SCNA-AA and SCNB-AA.

The wettability test is an easy method to verify the presence of chitosan on the surface and allows some predictions about the cellular response. Comparing the observed contact angles with the literature, a similar contact angle (around 76–80°) was registered on chitosan by Bumgarder et al. [37] and Ghanem and Katalinich [38]. On the other hand, these authors also reported a higher rate of protein absorption and osteoblast attachment on a coated surface with a lower contact angle. On the other hand, it was reported that a water contact angle of about 70° and a surface energy close to 40 mN/m is the threshold for cell attachment. Anti-adhesive surfaces are expected for wettability around this threshold [39] and tissue integration generally occurs on more hydrophilic surfaces, while more hydrophobic surfaces are cytotoxic [40].

3.3. Zeta potential titration curves

The zeta potential of the bare glasses and coated samples was measured as a function of the pH and the results are reported in Fig. 2. SCNA-TC-PBS and SCNB-TC-PBS were not measured because of the low surface coverage detected by SEM-EDS and FTIR analyses. The titration started at pH 5.6 and moved once toward the basic range and, then, once toward the acidic one (the same set of samples was used for the two titration ranges). A gap of the zeta potential around pH 5.5 can be observed in the curve when chemical reactions occurred during the first titration range (the basic one). Some measurements were interrupted before the end of the acidic titration because of the chitosan swelling and expansion of the coating. If the gap between the two samples closed because of the swelling, it was impossible to continue the measurement.

The isoelectric point (IEP) of the two glasses was close (Fig. 2a–c): at 2.66 for SCNA and 2.94 for SCNB. These values agreed with those reported in the literature for silica and silica-based glasses [41–43]. Such a low IEP was due to the abundance of acidic OH groups on both surfaces. A moderate increase in the IEP for SCNB glass can be associated with its higher sodium content, as reported in the literature [44]. Above IEPs, the zeta potential of the glasses was negative with an almost linear trend up to pH 4 for SCNA and 5 for SCNB. The higher the OH^- ions concentration was in the solution, the more numerous they were adsorbed

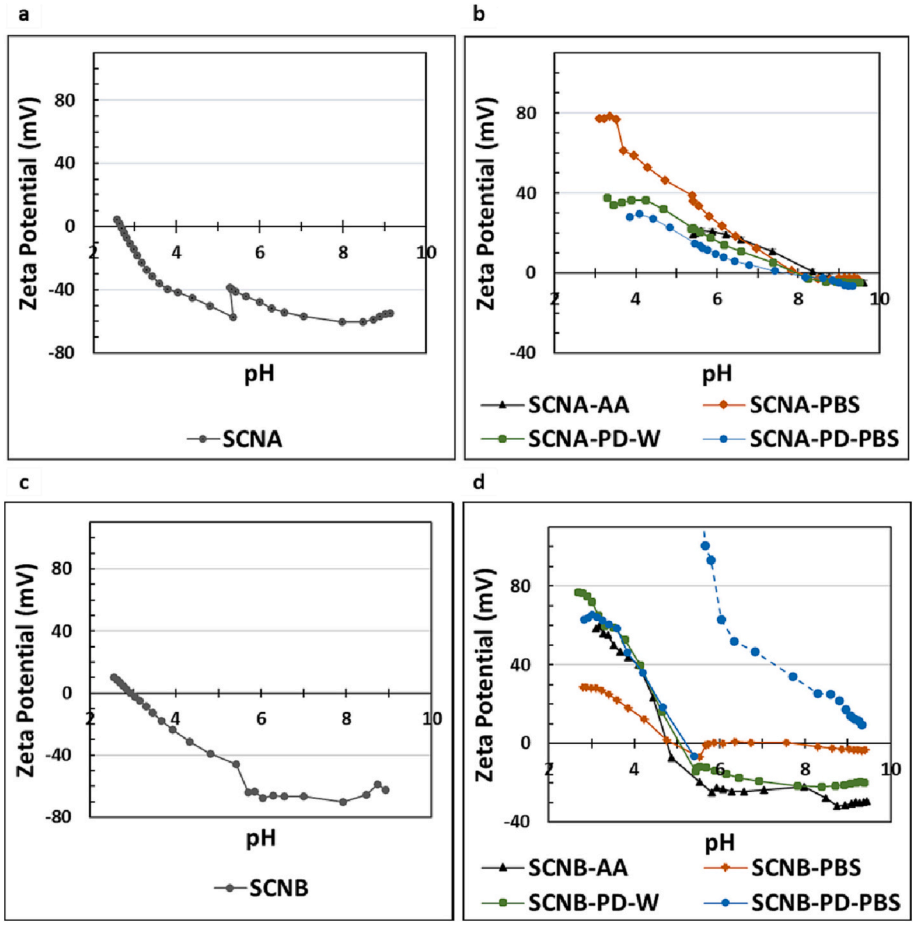

Fig. 2. Zeta potential titration curves of the bare SCNA and SCNB glasses (a and c) and of the chitosan-coated samples (b and d).

on the surface of the glasses replacing the adsorbed water molecules. The slope of the curve of SCNB was lower than the slope of SCNA in this range. This can be correlated to the higher wettability of SCNB and the lower amount of replaced water molecules by changing the pH of the electrolyte. This result agreed with the wettability data. There was a small gap of 18–20 mV at pH 5.6 in the titration curves of both bare glasses and it was close to the experimental error of the instrument in measuring the zeta potential. Both curves were almost flat in the range from pH 4 (SCNA) or pH 5 (SCNB) up to pH 8 showing a plateau. All hydroxyl groups of the surface were deprotonated above the onset of the plateau and no more ions were adsorbed from the solution even if it became more alkaline. The onset of the plateau is related to the pKa of the hydroxyl groups and SCNA showed OH groups with a slightly stronger acidic reactivity than SCNB. The difference in the IEPs agreed with the different onset of the plateau. The IEP of SCNA was lower (2.66 vs 2.94) because of the presence of OH groups with a stronger acidic reactivity. At pH higher than 8, the zeta potential increased on both glasses and the increase was due to the release of ions during the measurement and the reactivity of the glasses in an alkaline environment.

The coating of the glass surfaces with a chitosan layer caused a significant change in the titration curve (Fig. 2b–d). The isoelectric point of the SCNA-coated samples shifted to values above 7.5. The specific IEPs were 8.45 for SCNA-AA, 8.06 for SCNA-PBS, 7.93 for SCNA-PD-W, and 7.65 for SCNA-PD-PBS. The IEP obtained on SCNA-AA agreed with the value reported in the literature for chitosan [45] confirming a fully covered surface. The lower IEP of the other samples showed that the surface coverage was not complete, partially exposing the glass substrate. All standard deviations of the zeta potential on SCNA and SCNA coated samples were very low (lower than 5 mV) evidencing that the substrate and coatings were chemically and mechanically stable even under a liquid flux in a wide range of pH. Positive values of zeta potential in the acid range evidenced that protonated amino groups were exposed on the outermost layer of the chitosan coating and the positive charge in the acidic range moved from 10 mV on the glasses up to 80 mV on the coatings due to NH_3^+ groups. The exposure of a prevalence of amino groups by chitosan is not ubiquitous and it can strongly affect the biological outcome. When chitosan is in the form of a bulk hydrogel, it predominantly exposes the carboxylic groups with a low IEP (around 6) [46]. The physicochemical and biological properties of bulk chitosan cannot be transferred one-to-one to chitosan as a coating.

Fig. 2d shows the zeta potential titration curves of the coated SCNB samples. The detected IEPs were close to 5 (4.78–5.2). A shift toward the alkaline range with respect to the IEP of SCNB was evident, but discontinuous coatings can be supposed to be formed on this glass. The IEPs were at a value of pH between those expected for the glass substrate and chitosan because both materials were partially exposed on the surface. In the case of SCNB-PD-PBS, a gap of zeta potential was detected when the titration of the acidic range started because of the great reactivity of this surface. The standard deviation of zeta potential values measured in the whole alkaline range of this sample was above 35 mV, evidencing that this surface was unstable and the obtained data were not significant. In contrast, the standard deviations of SCNB-AA, SCNB-PBS, and SCNB-PD-W were between 5 and 10 mV indicating good stability of the coatings.

Concluding, the registered titration curves revealed relevant differences between the two bare glasses and among the coated samples. SCNA was less hydrophilic and it exposed on the surface OH groups with a stronger acid reactivity than SCNB. A large difference in zeta potential and strong electrostatic attraction can be expected in both cases between the glasses and chitosan due to deprotonated acidic OH groups on the

glasses and protonated amino groups on the chitosan. The surface coverage and/or chemical and mechanical stability of the coatings were not the same. A continuous and stable coating was present only on SCNA-AA, while all coated SCNB samples exposed a substantial amount of the glass substrate. The chitosan coating on SCNA predominantly exposed positive protonated amino groups in a wide range of pH (up to 7.5–8). All these features (high electrostatic attraction of the coating for the substrate, chemical and mechanical stability, predominance of a positive surface charge) can strongly affect the biological response of the bio-surface in contact with cells and physiological fluids.

3.4. Tape test

The adhesion of the coatings to the glass substrates was tested by a tape test. The presence/absence of the coating after the tape test was checked by SEM and EDS analysis. The results are reported in Fig. 3.

The adhesion of the chitosan coating on SCNA was robust as there was no peeling-off of the coating, outside the grid created with a blade, on SCNA-AA (classified as 5B – Fig. 3a) and very limited peeling-off occurred on SCNA-PBS, SCNA-PD-W, and SCNA-PD-PBS (classified as 4B - Fig. 3c-e-g).

In contrast, the chitosan coating was completely detached from SCNB-AA and SCNB-PD-PBS (classified as 0B – Fig. 3b–h), almost completely detached from SCNB-PD-W (classified as 1B - Fig. 3f), and only partially retained on SCNB-PBS (classified as 3B – Fig. 3d). This might be related to a reaction layer formed on the SCNB glass surface that was mechanically unstable and detached easily from the glass [47].

Data about SCNA-TC-PBS and SCNB-TC-PBS are not reported because the low surface coverage did not allow us to get quantitatively significant results. As a qualitative evaluation, the coating appeared to be firmly attached to the substrates, suggesting the positive effect of tresyl chloride surface activation on the mechanical adhesion.

3.5. Bioactivity (in vitro precipitation of hydroxylapatite)

The bioactivity of the bare glasses and some coated samples was tested by soaking in SBF for 14 days. According to the previous results, the samples coated by direct physical attachment in acetic acid and by using polydopamine as a linker (in water) were selected for this test. The SEM images of the soaked samples are reported in Fig. 4.

The typical morphology of hydroxylapatite crystals was not detected on SCNA (Fig. 4a) because this glass was not reactive enough to show bioactivity within fourteen days of soaking. Some small areas with some precipitates were observed on the surface of the SCNA-soaked sample; the area covered by hydroxylapatite crystals was about 5 %.

In contrast, the surface of SCNB was fully covered by hydroxylapatite crystals after soaking (Fig. 4b) as expected considering the absence of alumina and the high reactivity of this glass [27]. Hydroxylapatite had a morphology with rod-like crystals and dendritic agglomerates as already reported in the literature [48].

The SEM images of SCNA-AA and SCNB-AA after soaking are reported in Fig. 4c–d. No evident formation of hydroxylapatite was visible on SCNA-AA while some residues of the chitosan coating still covered the surface. In contrast, SCNB-AA was fully covered by hydroxylapatite with a typical cauliflower morphology [49,50] without any sign of the chitosan coating. Similar results were obtained for SCNA-PD-W and SCNB-PD-W (Fig. 4e–f). The main difference was the reduced presence of the chitosan coating residues on SCNA-PD-W compared to SCNA-AA.

In conclusion, SCNA coated with chitosan by physical attachment in acetic acid was a system with full surface coverage and high mechanical and chemical stability, even during soaking in an aqueous medium. This suggests applications where the chitosan effect on the surface must be retained for several days. In contrast, SCNB could be fully covered by chitosan by physical attachment in acetic acid and showed fast bioactivity that was not hindered by the chitosan coating. In this case, the coating can be quickly desorbed and, hence, the SCNB-coated glass is of interest for short-time applications and fast surface reactions.

3.6. Preliminary biological testing

3.6.1. Cell and culture morphology by epifluorescence

Epifluorescence of RAW 264.7 macrophage cells on day 1 of culture (Fig. 5, left panel, a–c) revealed their predominantly rounded shape when grown on the SCNA-AA surface (Fig. 5c, arrow). These cells were less spread out than those grown on control SCNA – which occasionally also showed elongated shapes (Fig. 5a, arrowheads) –, and initially interacted with each other to form three-dimensional cellular clusters/aggregates (Fig. 5b–c). Osteopontin labeling was restricted to the perinuclear region in cells grown on both surfaces (Fig. 5a–c). The morphology of RAW 264.7 cells on SCNA-AA reflected the ability of cells to self-organize on a non-adhesive surface by forming bonds with adjacent cells to maximize cohesive strength, as demonstrated elsewhere [51,52]. In addition, the absence of elongated macrophage phenotypes during the initial interactions of RAW 264.7 cultures with SCNA-AA was indicative of the occurrence of non-activated M0 and/or pro-inflammatory M1 states [53] reviewed [54], a finding that should be further molecularly characterized.

On day 3 of culture, UMR-106 osteoblastic cells spread over the control SCNA and the peripheral area of SCNA-AA surfaces and were sub-confluent, showing polygonal shapes and cell-cell contacts (Fig. 5d–e). The grafting of PDC on SCNA-AA dramatically reduced cell number on the main central part of the disc surface, where three-dimensional spheroid-like cellular structures were occasionally observed (Fig. 5f, arrow and inset). Bone sialoprotein labeling was

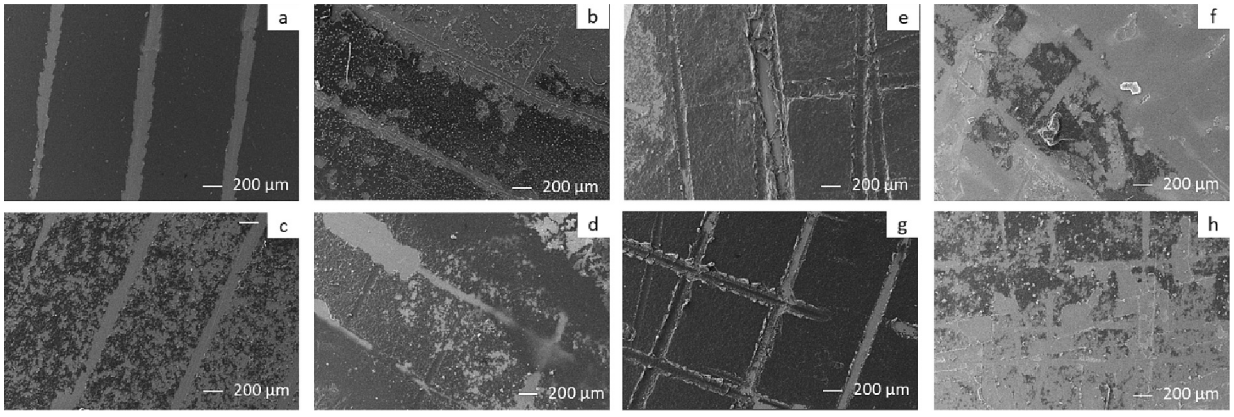

Fig. 3. SEM images of the coated samples after the tape test: (a) SCNA-AA, (b) SCNB-AA, (c) SCNA-PBS, (d) SCNB-PBS, (e) SCNA-PD-W, (f) SCNB-PD-W, (g) SCNA-PD-PBS, (h) SCNB-PD-PBS.

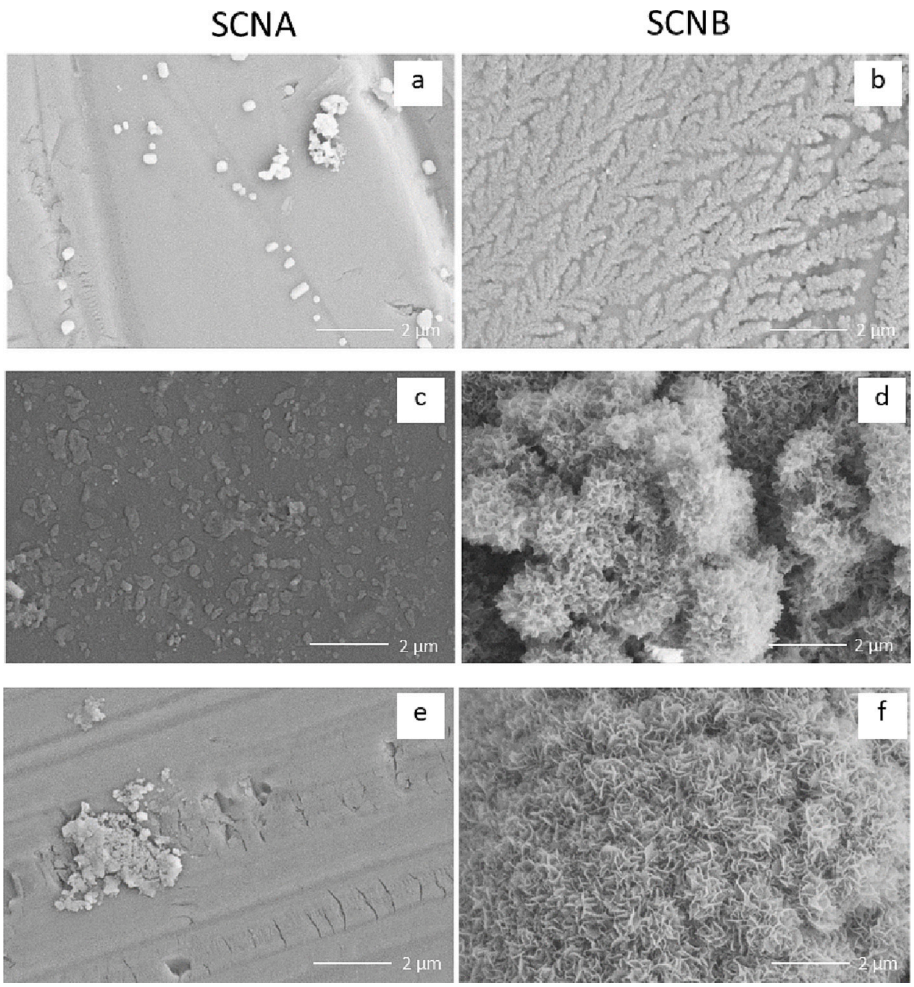

Fig. 4. SEM micrographs of the samples soaked for 14 days in SBF: (a) SCNA; (b) SCN; (c) SCNA-AA; (d) SCNB-AA; (e) SCNA-PD-W; (f) SCNB-PD-W.

limited to a paranuclear region in cells on both surfaces, including those forming spheroid-like structures (Fig. 5, d–f). The morphological results of UMR-106 cell response to SCNA-AA suggested that this surface was non-adhesive for pre-osteoblastic cells, although no significant changes in terms of cell viability and osteogenic potential compared with SCNA were detected (see below). While the presence of chitin derivatives, such as chitosan, has the potential to modulate the immunoinflammatory response during the early stages of tissue repair around implants [55], their non-adhesiveness (for diverse cell types) when used as surface coatings might contribute to the development of devices for clinical situations in which the osseointegration phenomenon is not desirable [39], as is the case for plates and screws for temporary fracture fixation. In addition, PDC coatings could be exploited in in-vitro studies of tumor biology, as they support the formation of three-dimensional multicellular spheroids that have been shown to mimic key features of malignant solid tumors in vivo [56]. Different results are reported in the literature in the case of pre-incubation of chitosan into culture media or serum which are able to increase cell adhesion [57].

3.6.2. Cell metabolic activity/cell viability assay

The results of the MTT assay are shown in Fig. 5 (upper right panel for RAW 264.7 macrophage cells, and lower right panel for UMR-106 osteoblastic cells). For RAW 264.7 cells, the lowest values were observed on hour 6 of culture on SCNA and SCNA-AA surfaces, with a significant increase on day 3 of culture only for SCNA. Irrespective of the time point, there were no significant differences between surfaces, despite a tendency toward lower values for SCNA-AA on day 3 of culture. Similarly, UMR-106 cell viability did not alter on both surfaces.

3.6.3. Mineralization of osteoblastic cell cultures

Alizarin Red staining revealed no significant differences between surfaces on day 7 of UMR-106 cell cultures, despite a tendency toward tripling of the calcium content for SCNA-AA (Fig. 5, lower right panel).

In conclusion, these preliminary results are interesting because, firstly, they confirmed that the chitosan coating was still present on the SCNA glass during the initial days of cell culture and it made a difference in the biological response of macrophages and osteoblastic cells. Secondly, wettability results suggested that low cell adhesion on the coated surface could occur, a hypothesis that was confirmed by the UMR 106 cell culture. The results of cell viability and mineralization confirmed that cytotoxicity, if any, was limited and that the adherent cells were viable and functional.

4. Conclusion

Chitosan coatings were successfully deposited on two bioactive glasses with different reactivity. The coating features were affected by the chemical composition of the glasses and the coating procedures. Almost complete surface coverage was achieved by using direct physical attachment (in acetic acid) or polydopamine (larger in PBS), while direct physical attachment in PBS halved the covering, and surface activation with tresyl chloride dropped it to one-quarter on both glasses. The chitosan coating had a contact angle of about 80° when it was smooth and continuous (SCNA-AA).

The coatings on SCNA were chemically and mechanically stable (classified as 4-5B by tape tests, partially maintained after soaking for 14 days in the case of SCNA-AA). On SCNA, the coatings had an

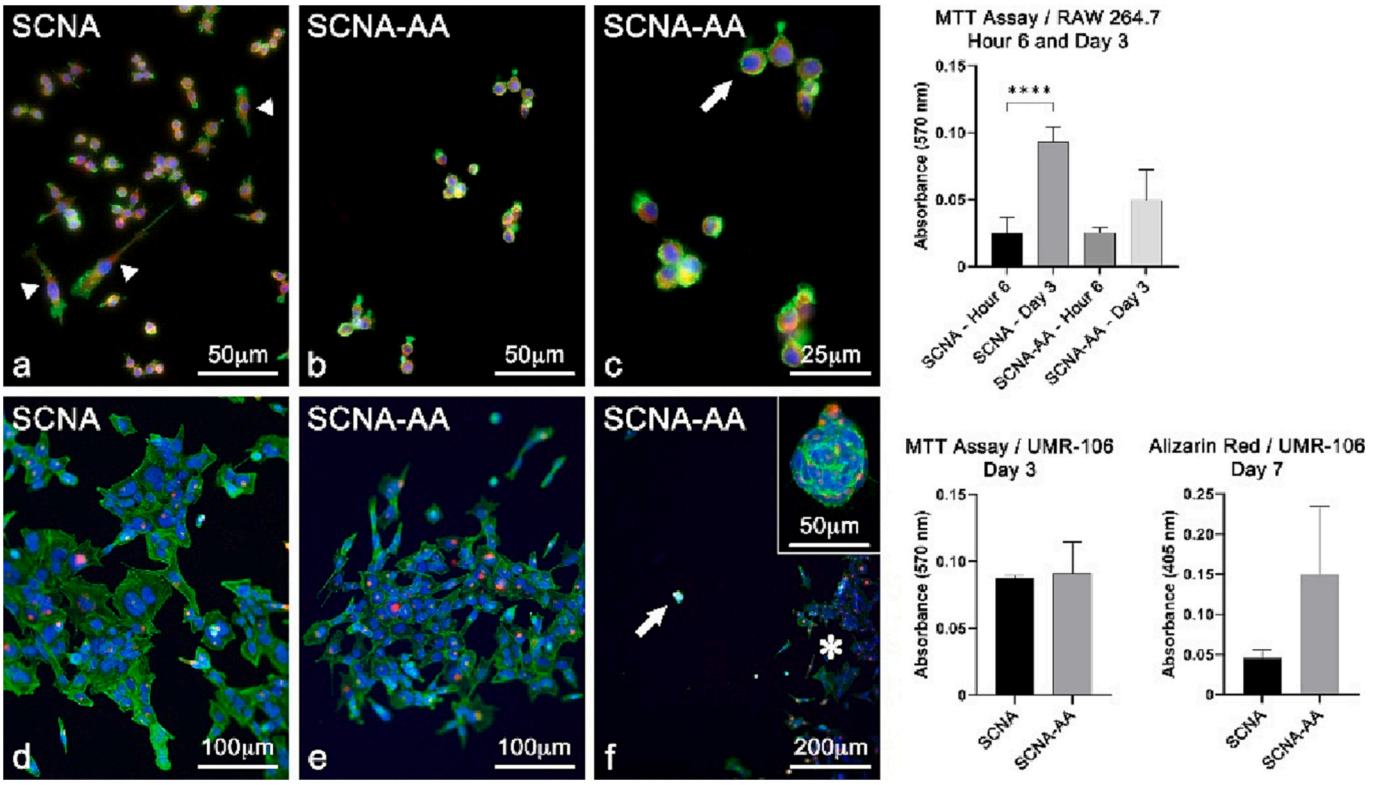

Fig. 5. Left panel – Epifluorescence of RAW 264.7 macrophage (a–c) and UMR-106 osteoblastic (d–f) cell cultures grown on control SCNA (a, d) and PDC-coated SCNA-AA (b, c, e, and f) surfaces on days 1 (a–c) and 3 (d–f) of culture. Green fluorescence, actin cytoskeleton; red fluorescence, osteopontin (a–c) or bone sialoprotein (d–f) labeling; blue fluorescence, cell nuclei. The majority of RAW 264.7 cells exhibit roundish shapes on SCNA (a) and SCNA-AA (b, c, and arrow in c). However, on SCNA some of them are clearly elongated (A arrowheads). UMR-106 cells show spread polygonal shapes on SCNA (d) and peripheral area of SCNA-AA (e, f asterisk) surfaces. On focal areas of the central part of the SCNA-AA disc surface, UMR-106 cells interacted with each other to form three-dimensional spheroid-like structures (F, arrow and inset). Osteopontin (a–c) and bone sialoprotein (d–f) labelings were cytoplasmic. Upper right panel – Cell metabolic activity/cell viability (MTT assay, optical density, mean and standard deviation) of RAW 264.7 macrophage cell cultures grown on SCNA and SCNA-AA at 6 h and 3 days of culture (****$p < 0.0001$). Lower right panel – Cell metabolic activity/cell viability (MTT assay, optical density, median and interquartile range) of UMR-106 osteoblastic cell cultures grown on SCNA and SCNA-AA at 3 days of culture ($p = 0.68$). Alizarin Red assay (optical density, mean and standard deviation) of UMR-106 osteoblastic cell cultures grown on SCNA and SCNA-AA at day 7 of culture ($p = 0.0505$).

isoelectric point around 8 and clearly showed a prevalence of protonated amino groups on the outermost layer. SCNA-AA is of interest for applications where the chitosan effect on the surface must be retained for several days, as confirmed by the biological results. The coating affected the biological outcome of SCNA-AA with M1 polarization (1 day) and a tendency toward reduced viability of macrophages (3 days), while osteoblastic cells showed poor adhesion (in agreement with wettability) but good viability and functionality (3–7 days).

In contrast, SCNB could be fully covered by chitosan in the case of SCNB-AA. All coatings on SCNB were chemically and mechanically unstable (classified as 0-3B by tape tests, dissolved during soaking as observed on SCNB-AA and SCNB-PD-W) but preserved their bioactivity. SCNB-AA is of potential interest for its effect on a short time frame and fast surface reaction and bioactivity.

Ethical approval

No ethical approval by any institutional review board or ethics committee was needed because no experiment involving human tissue or animals was carried on.

CRediT authorship contribution statement

S. Spriano: Conceptualization, Funding acquisition, Methodology, Project administration, Supervision, Writing – original draft. **G. Riccucci:** Investigation. **G. Örlygsson:** Conceptualization, Funding acquisition, Methodology, Supervision, Writing – original draft, Writing – review & editing. **C.H. Ng:** Conceptualization, Funding acquisition, Methodology, Supervision, Writing – original draft, Writing – review & editing. **E. Vernè:** Conceptualization, Supervision, Writing – review & editing. **F.P. Sehn:** Investigation. **P.T. de Oliveira:** Conceptualization, Funding acquisition, Methodology, Supervision, Writing – original draft, Writing – review & editing. **S. Ferraris:** Conceptualization, Investigation, Methodology, Supervision, Writing – original draft, Writing – review & editing.

Declaration of competing interest

The authors declare that they have no known competing financial interests or personal relationships that could have appeared to influence the work reported in this paper.

Data availability

No data was used for the research described in the article.

Acknowledgments

European Commission, Ministero dell'Università e della Ricerca (MUR), and the Icelandic Technology Development Fund (agreement no. 169010-0613) are acknowledged for funding the NAT4MORE project (M.ERA-NET 2016).

This research was also partially funded by the National Council for Scientific and Technological Development (CNPq, Brazil - grant number 315266/2020-1 - scholarship on research productivity to P.T.d.O.), the State of São Paulo Research Foundation (FAPESP, Brazil - grant number 2016/50298-4 - regular project to P.T.d.O.), and the Coordenação de Aperfeiçoamento de Pessoal de Nível Superior (CAPES, Brazil - postdoc scholarship to F.P.S.).

Politecnico di Torino is acknowledged for supporting open-access publication.

Appendix A. Supplementary data

Supplementary data to this article can be found online at https://doi.org/10.1016/j.surfcoat.2023.129824.

References

[1] L.L. Hench, J.M. Polak, Third-generation biomedical materials, Science 295 (2002) 1014–1017.
[2] M. Montazerian, E.D. Zanotto, A guided walk through larry hench's monumental discoveries, J. Mater. Sci. 52 (2017) 8695–8732.
[3] K. Ohura, T. Yamamuro, T. Nakamura, T. Kokubo, Y. Ebisawa, Y. Kotoura, M. Oka, Bone-bondingability of P_2O_5-free CaO-SiO_2 glasses, J. Biomed. Mater. Res. 25 (1991) 357–365.
[4] F. Hyunmin Kim, T. Miyaji, C. Ohtsuki Kokubo, Takashi Nakamura, Bioactivity of Na_2O-CaO-SiO_2 glasses, J. Am. Ceram. Soc. 78 (1995) 2405–2411.
[5] E. Verne, E. Bona, E. Angelini, F. Rosalbino, P. Appendino, Correlation between microstructure and properties of biocomposite coatings, J. Eur. Ceram. Soc. 22 (2002) 2315–2323.
[6] E. Verne, S. Di Nunzio, M. Bosetti, P. Appendino, C. Vitale Brovarone, G. Maina, M. Cannas, Surface characterization of silver-doped bioactive glass, Biomaterials 26 (2005) 5111–5119.
[7] S. Kumari, H.R. Tiyyagura, Y.B. Pottathara, K.K. Sadasivuni, D. Ponnamma, T.E. L. Douglas, A.G. Skirtach, M.K. Mohan, Surface functionalization of chitosan as a coating material for orthopaedic applications: a comprehensive review, Carbohydr. Polym. 255 (2021), 117487.
[8] D. Zhao, S. Yu, B. Sun, S. Gao, S. Guo, K. Zhao, Biomedical applications of chitosan and its derivative nanoparticles, Polymers 10 (4) (2018) 462.
[9] F. Seidi, M.K. Yazdi, M. Jouyandeh, M. Dominic, H. Naeim, M.N. Nezhad, B. Bagheri, S. Habibzadeh, P. Zarrintaj, M.R. Saeb, M. Mozafari, Review: chitosan-based blends for biomedical applications, Int. J. Biol. Macromol. 183 (2021) 1818–1850.
[10] H. Hamedi, S. Moradi, S.M. Hudson, A.E. Tonelli, M.W. King, Chitosan based bioadhesives for biomedical applications: a review, Carbohydr. Polym. 282 (2022), 119100.
[11] G. Örlygsson, E.H. Laxdal, S. Kárason, A. Dagbjartsson, E. Gunnarsson, C.H. Ng, J. M. Einarsson, J. Gíslason, H.J. Jónsson, Mineralization in a critical size bone-gap in sheep tibia improved by a chitosan-calcium phosphate-based composite as compared to predicate device, Materials 15 (3) (2022) 838.
[12] S. Chang, Y. Lin, G. Wu, C. Huang, G.J. Tsa, Effect of chitosan molecular weight on anti-inflammatory activity in the RAW 264.7 macrophage model, Int. J. Biol. Macromol. 131 (2019) 167–175.
[13] V.N. Davydova, I.V. Sorokina, A.V. Volod'ko, E.V. Sokolova, M.S. Borisova, I. M. Yermak, The comparative immunotropic activity of carrageenan, chitosan and their complexes, Mar. Drugs 18 (9) (2020) 458–495.
[14] R. Cao, H. Yu, H. Long, H. Zhang, C. Hao, L. Shi, Y. Du, S. Jiao, A. Guo, L. Ma, Z. Wang, Low deacetylation degree chitosan oligosaccharide protects against IL-1β induced inflammation and enhances autophagy activity in human chondrocytes, J. Biomater. Sci. Polym. Ed. 33:(4) (2022) 517–531.
[15] A. Oberemko, A.M. Salaberria, R. Saule, G. Saulis, M. Kaya, J. Labidi, V. Baublys, Physicochemical and in vitro cytotoxic properties of chitosan from mushroom species (*Boletus bovinus* and *Laccaria laccata*), Carbohydr. Polym. 221 (2019) 1–9.
[16] Y. Pang, A. Qin, X. Lin, L. Yang, Q. Wang, Z. Wang, Z. Shan, S. Li, J. Wang, S. Fan, Q. Hu, Biodegradable and biocompatible high elastic chitosan scaffold is cell-friendly both in vitro and in vivo, Oncotarget 8 (22) (2017) 35583–35591.
[17] M.H. Ho, C.J. Yao, M.H. Liao, P.I. Lin, S.H. Liu, R.M. Chen, Chitosan nanofiber scaffold improves bone healing via stimulating trabecular bone production due to upregulation of the Runx2/osteocalcin/alkaline phosphatase signaling pathway, Int. J. Nanomedicine 10 (2015) 5941–5954.
[18] S.P. Soundarya, A.H. Menon, S.V. Chandran, N. Selvamurugan, Bone tissue engineering: scaffold preparation using chitosan and other biomaterials with different design and fabrication techniques, Int. J. Biol. Macromol. 119 (2018) 1228–1239.
[19] V.M. Rusu, C.H. Ng, M. Wilke, B. Tiersch, P. Fratzl, M.G. Peter, Size-controlled hydroxyapatite nanoparticles as self-organized organic–inorganic composite materials, Biomaterials 26 (26) (2005) 5414–5426.
[20] R.A.A. Muzzarelli, Review: chitins and chitosans for the repair of wounded skin, nerve, cartilage and bone, Carbohydr. Polym. 76 (2) (2009) 167–182.
[21] E. Vernè, M. Miola, C. Vitale Brovarone, M. Cannas, S. Gatti, G. Fucale, et al., Surface silver-doping of biocompatible glass to induce antibacterial properties. Part I: massive glass, J. Mater. Sci. Mater. Med. 20 (3) (2009) 733–740.
[22] M. Miola, S. Ferraris, S. Di Nunzio, P.F. Robotti, G. Bianchi, G. Fucale, et al., Surface silver-doping of biocompatible glass to induce antibacterial properties. Part II: plasma sprayed glass-coatings, J. Mater. Sci. Mater. Med. 20 (3) (2009) 741–749.
[23] E. Verné, S. Ferraris, C. Vitale-Brovarone, S. Spriano, C.L. Bianchi, A. Naldoni, M. Morra, C. Cassinelli, Alkaline phosphatase grafting on bioactive glasses and glass ceramics, Acta Biomater. 6 (2010) 229–240.
[24] E. Vernè, C. Vitale-Brovarone, E. Bui, C.L. Bianchi, A.R. Boccaccini, Surface functionalization of bioactive glasses, J. Biomed. Mater. Res. 90 (2009) 981–992, https://doi.org/10.1002/jbm.a.32153.
[25] X. Zhang, S. Ferraris, E. Prenesti, E. Verné, Surface functionalization of bioactive glasses with natural molecules of biological significance, part I: gallic acid as model molecule, Appl. Surf. Sci. 287 (2013) 329–340.
[26] X. Zhang, S. Ferraris, E. Prenesti, E. Verné, Surface functionalization of bioactive glasses with natural molecules of biological significance, part II: grafting of polyphenols extracted from grape skin, Appl. Surf. Sci. 287 (2013) 341–348.
[27] S. Ferraris, I. Corazzari, F. Turci, A. Cochis, L. Rimondini, E. Vernè, Antioxidant activity of silica-based bioactive glasses, ACS Biomater. Sci. Eng. 7 (2021) 2309.
[28] S. Ferraris, I. Corazzari, F. Turci, A. Cochis, L. Rimondini, S. Spriano, J. Massera, E. Vernè, Surface properties and antioxidant activity of silicate and borosilicate bioactive glasses, Adv. Eng. Mater. 25 (2022), 2200978.
[29] P.J. Potts, A Handbook of Silicate Rock Analysis, Springer, Dordrecht, 1987.
[30] ASTM D3359-17, Standard Methods for Rating Adhesion by Tape Test, ASTM International, West Conshohocken, PA, 2017.
[31] T. Kokubo, H. Takadama, How useful is SBF in predicting in vivo bone bioactivity? Biomaterials 27 (15) (2006) 2907–2915.
[32] L.R. Zuardi, F.S. de Oliveira, R.R. Fernandes, M.P.O. Gomes, S. Spriano, A. Nanci, P.T. de Oliveira, Effects of rmBMP-7 on osteoblastic cells grown on a nanostructured titanium surface, Biomimetics 7 (2022) 136, https://doi.org/10.3390/biomimetics7030136.
[33] A.S. Martorano, N.S. Messias, R.L. Bighetti-Trevisan, P.T. de Oliveira, L.M.S. de Castro Raucci, Neto W. Raucci, In vitro inflammatory modulation of bioceramic endodontic sealer in macrophages stimulated by bacterial lipopolysaccharide, Int. Endod. J. 56 (2) (2023) 213–226, https://doi.org/10.1111/iej.13858.
[34] J. Moura, L.N. Teixeira, C. Ravagnani, O. Peitl, E.D. Zanotto, M.M. Beloti, H. Panzeri, A.L. Rosa, P.T. de Oliveira, In vitro osteogenesis on a highly bioactive glass-ceramic (Biosilicate), J. Biomed. Mater. Res. A 82 (3) (2007) 545–557, https://doi.org/10.1002/jbm.a.31165.
[35] R.C.P. Scannavino, G. Riccucci, S. Ferraris, G.L.C. Duarte, P.T. de Oliveira, S. Spriano, Functionalization with polyphenols of a nano-textured Ti surface through a high-amino acid medium: a chemical-physical and biological characterization, Nanomaterials 12 (17) (2022) 2916, https://doi.org/10.3390/nano12172916.
[36] C.A. Gregory, W.G. Gunn, A. Peister, D.J. Prockop, An Alizarin red-based assay of mineralization by adherent cells in culture: comparison with cetylpyridinium chloride extraction, Anal. Biochem. 329 (1) (2004) 77–84, https://doi.org/10.1016/j.ab.2004.02.002.
[37] J.D. Bumgardner, R. Wiser, S.H. Elder, R. Jouett, Y. Yang, J.L. Ong, et al., Contact angle, protein adsorption and osteoblast precursor cell attachment to chitosan coatings bonded to titanium, Aust. J. Biol. Sci. 14 (12) (2012) 1401–1409.
[38] A. Ghanem, M. Katalinich, Characterization of chitosan films for tissue, Appl. Bionics Biomech. 2 (1) (2005) 9–16.
[39] F. Gamna, A. Cochis, A.C. Scalia, A. Vitale, S. Ferraris, L. Rimondini, S. Spriano, The use of vitamin E as an anti-adhesive coating for cells and bacteria for temporary bone implants, Surf. Coat. Technol. 444 (2022), 128694, https://doi.org/10.1016/j.surfcoat.2022.128694.
[40] J.O. Hollinger, An Introduction to Biomaterals, second ed., 2011.
[41] M. Kosmulsky, pH-dependent surface charging and points of zero charge. IV. Update and new approach, Colloid Interface Sci. 337 (2009) 439–448.
[42] M. Cazzola, I. Corazzari, E. Prenesti, E. Bertone, E. Vernè, S. Ferraris, Bioactive glass coupling with natural polyphenols: surface modification, bioactivity and anti-oxydant ability, Appl. Surf. Sci. 367 (2016) 237–248.
[43] S. Spriano, Chandra V. Sarath, A. Cochis, F. Uberti, L. Rimondini, E. Bertone, A. Vitale, C. Scolaro, M. Ferrari, F. Cirisano, G. Gautier di Confiengo, S. Ferraris, How do wettability, zeta potential and hydroxylation degree affect the biological response of biomaterials? Mater. Sci. Eng. C 74 (2017) 542–555.
[44] M.J. Owen, P.R. Dvornie, Silicon Surface Science, Springer, 2012.
[45] Z. Bujnakova, E. Dutkova, A. Zorkovska, E. Al, Mechanochemical synthesis and in vitro studies of chitosan-coated InAs/ZnS mixed nanocrystals, J. Mater. Sci. 52 (2017) 721–735.
[46] R. Sesia, S. Ferraris, M. Sangermano, S. Spriano, UV-cured chitosan-based hydrogels strengthened by tannic acid for the removal of copper ions from water, Polymers 14 (2022) 4645, https://doi.org/10.3390/polym14214645.
[47] S. Ferraris, S. Yamaguchi, N. Barbani, C. Cristallini, G. Gautier di Confiengo, J. Barberi, M. Cazzola, M. Miola, E. Vernè, S. Spriano, The mechanical and chemical stability of the interfaces in bioactive materials: the substrate-bioactive surface layer and hydroxyapatitebioactive surface layer interfaces, Mater. Sci. Eng. C 116 (2020), 111238.
[48] S. Rehman, K. Khan, M. Mujahid, S. Nosheen, Synthesis of nano-hydroxyapatite and its rapid mediated surface functionalization by silane coupling agent, Mater. Sci. Eng. C 58 (2016) 675–681, https://doi.org/10.1016/j.msec.2015.09.014.
[49] J. Lin, T. Tsai, W. Say, C. Chiu, S. Chen, In vitro study of electrodeposited fluoridated hydroxyapatite coating on G-II titanium with a nanostructured TiO_2 interlayer, Biomed. Mater. 12 (2017), 025018.
[50] S. Bharati, M.K. Sinha, D. Basu, Hydroxyapatite coating by biomimetic method on titanium alloy using concentrated SBF, Bull. Mater. Sci. 28 (6) (2005) 617–621.

[51] S. Douezan, F. Brochard-Wyart, Active diffusion-limited aggregation of cells, Soft Matter 8 (2012) 784–788, https://doi.org/10.1039/C1SM06399E.
[52] D. Mukhopadhyay, R. De, Aggregation dynamics of active cells on non-adhesive substrate, Phys. Biol. 16 (4) (Jun 4, 2019), 046006, https://doi.org/10.1088/1478-3975/ab1e76.
[53] F.Y. McWhorter, T. Wang, P. Nguyen, T. Chung, W.F. Liu, Modulation of macrophage phenotype by cell shape, Proc. Natl. Acad. Sci. U. S. A. 110 (43) (2013) 17253–17258, https://doi.org/10.1073/pnas.1308887110.
[54] R. Sridharan, B. Cavanagh, A.R. Cameron, D.J. Kelly, F.J. O'Brien, Material stiffness influences the polarization state, function and migration mode of macrophages, Acta Biomater. 89 (2019) 47–59, https://doi.org/10.1016/j.actbio.2019.02.048.
[55] S. Ferraris, G. Örlygsson, C.H. Ng, G. Riccucci, S. Spriano, Chemical, physical, and mechanical characterization of chitosan coatings on a chemically pre-treated Ti6Al4V alloy, Surf. Coat. Technol. 15 (441) (2022), 128571, https://doi.org/10.1016/j.surfcoat.2022.128571.
[56] A. Kamatar, G. Gunay, H. Acar, Natural and synthetic biomaterials for engineering multicellular tumor spheroids, Polymers 12 (11) (2020) 2506, https://doi.org/10.3390/polym12112506.
[57] S.-H.-M. Wong, S.-S. Lim, T.-J. Tiong, P.-L. Show, H.-F.-M. Zaid, H.-S. Loh, Preliminary in vitro evaluation of chitosan–graphene oxide scaffolds on osteoblastic adhesion, proliferation, and early differentiation, Int. J. Mol. Sci. 21 (15) (2020) 5202, https://doi.org/10.3390/ijms21155202.